

Thermal Stability of FeS₂ Cathode Material in “Thermal” Batteries: Effect of Dissolved Oxides in Molten Salt Electrolytes

Patrick J. Masset

Karl Winnacker Institut der Dechema e. V., Theodor-Heuss Allee 25, D-60486 Frankfurt am Main, Germany

Reprint requests to P.J. M.; Fax: +49 69 7564-362/388; E-mail: masset@dechema.de

Z. Naturforsch. **63a**, 596–602 (2008); received March 4, 2008

Presented at the EUCHEM Conference on Molten Salts and Ionic Liquids, Hammamet, Tunisia, September 16–22, 2006.

The thermal stability of FeS₂ cathode material for thermal batteries is investigated in the LiCl-KCl eutectic containing up to 10 wt% Li₂O (used as anti-peak). The results show that the decomposition of pyrite shifts to higher temperatures in the presence of molten salts as the S₂ gas is repressed by the liquid phase. For high lithium oxide contents the decomposition temperature of pyrite decreases by 100 °C. In addition Li₂FeS₂ as reaction product is evidenced whereas Li₃Fe₂S₄ is expected from literature data.

Key words: Thermal Batteries; Electrolyte; Pyrite; Oxide; Molten Salt; LiCl-KCl Eutectic.

1. Introduction

The development of thermally activated batteries (“thermal batteries”) is accredited to the German scientists who developed these generators during world war II for the V2 rockets [1]. The first batteries used exhaust heat from the rocket to keep the electrolyte molten in the battery during the missile’s mission. This technology was brought back to the United States in 1946. The new technology was immediately adapted to replace the previous batteries because of intrinsic advantages [1]. Thermal batteries are primary batteries that use molten salts as electrolytes [2] and employ the heat internal pyrotechnic sources to bring the battery stack to operating temperatures. As cathode material pyrite, FeS₂, is now commonly used; its thermal stability has been widely investigated under inert or corrosive atmosphere by non-isothermal or isothermal analyses [3]. During its thermal decomposition, pyrite is transformed progressively into pyrrhotite, FeS_{1.14}, and the FeS₂ grains become porous as sulfur gas escapes. The mechanism of FeS₂ and FeS_{1.14} thermal decomposition was investigated and modeled by Hoare et al. [4]. However, the thermal behaviour of pyrite in molten salts is less investigated. Pyrite as well as the pyrrhotite dissolve partially in molten salts at high temperature. The predominance

diagram in the LiCl-KCl eutectic was provided by Santarini [5] which stated that the solubility limit of Li₂S is lower than in other studies due to the formation of the so-called J-phase (general composition K_{5.5}Li_{0.6}Fe₂₄S_{25.9}Cl_{1.0} [6, 7]) that forms between FeS₂ and the LiCl-KCl eutectic above 470 °C [8–10]. The decomposition kinetics of FeS₂ in molten salts has been little investigated by Barlow [11], who reported the thermal stability of pyrite in the molten LiCl-KCl and LiF-LiCl-LiBr eutectics. More recently Masset et al. [12, 13] measured the thermal decomposition kinetics in LiX-KX (X = Cl, Br, I) mixtures, in the LiF-LiCl-LiI and LiF-LiCl-LiBr electrolytes. In many cases the weight variations varied linearly with time.

Experimentally, sulfate crystal growth has been evidenced by XPS measurements on a fresh pyrite surface in vacuum [14]. The thermal decomposition of sulfates leads to the formation of Fe₂O₃ [15]. A large voltage transient (“spike”) occurs upon activation of a thermal battery if FeS₂ contains impurities such as oxides, sulfates, and elemental sulfur or if the activity of Li is not fixed in the cathode. This is overcome by lithiation of the catholyte [16–19] using Li₂O or Li₂S lithiation agents in small quantities of 1–2 wt% although the Li₂O solubility in the molten salts is far lower [20–24]. Oxides or hydroxides may arise from the hydrolysis of the salt if this latter is not correctly dried.

According to the quaternary phase diagram Li-Fe-S-O [25, 26], the reaction pathway leads to the formation of Li₃Fe₂S₄ by adding Li₂O to the pyrite. However, the influence of hydroxides or oxides dissolved in the electrolyte on the chemical stability of pyrite has poorly been investigated. The aim of this work was to determine the thermal stability of pyrite in the LiCl-KCl eutectic in the presence of dissolved oxides.

2. Experimental

2.1. Salt Preparation

LiCl and KCl were purchased from Sigma-Aldrich (99.99% purity). Lithium oxide, Li₂O (100 mesh), used in the cathode mixture came from Cerac. The salts were dried individually under vacuum in a quartz crucible for 15 h at 200 °C. The mixtures were fused under argon in a glassy carbon crucible maintained at 500 °C for 15 h. They were quenched directly in the grinder. Once ground, they were stored in a glove box under argon atmosphere.

2.2. Techniques

Differential scanning calorimetry (DSC) experiments were performed using a Setaram 111 thermal analyzer. Experiments were carried out in a dynamic atmosphere (flow rate of 125 l h⁻¹) of dry argon (less than 1 ppm H₂O) on 150 mg samples. The crucibles were made of alumina, Al₂O₃. The samples were heated from 30 to 800 °C at 3 °C min⁻¹.

The sample oxygen content was measured by means of carbothermal reduction oxide analysis. Experiments were carried out with a LECO TC-436 instrument. Oxygen of the sample reacts with the carbon crucible to produce carbon monoxide. This operates at high temperature and short time. Thus, CO is transformed in CO₂ by oxidation in a CuO tower. Finally, the CO₂ level is detected by an infrared cell. The specimens were prepared in glove box and the sample weight was close to 1 mg.

Microstructural features of the starting materials were determined by using a JEOL scanning electron microscope. Semi-quantitative determinations of the composition were carried out by energy dispersive analysis of X-rays (EDAX) on the EDS system attached to the JEOL scanning electron microscope. No thin films of gold on the exposed surfaces were applied before microscopic viewing; samples were sufficiently

electrical conductive and no electrostatic charging was noticed.

X-Ray diffraction (XRD) was performed on a Siemens 5000 diffractometer. The samples were prepared in a glove box and covered with polyethylene film in order to limit the reaction of the samples with the atmosphere during the analysis.

3. Results and Discussion

3.1. Materials Characterization

Impurity concentrations (mainly oxides and/or hydroxides) were measured by titration and were found to be less than 10⁻⁴ in the molar fraction scale. By means of DSC the melting point of the electrolytes was measured and found to be close to (354 ± 3) °C. The obtained value was found similar to previous values already reported in the literature (352 °C [27, 28]).

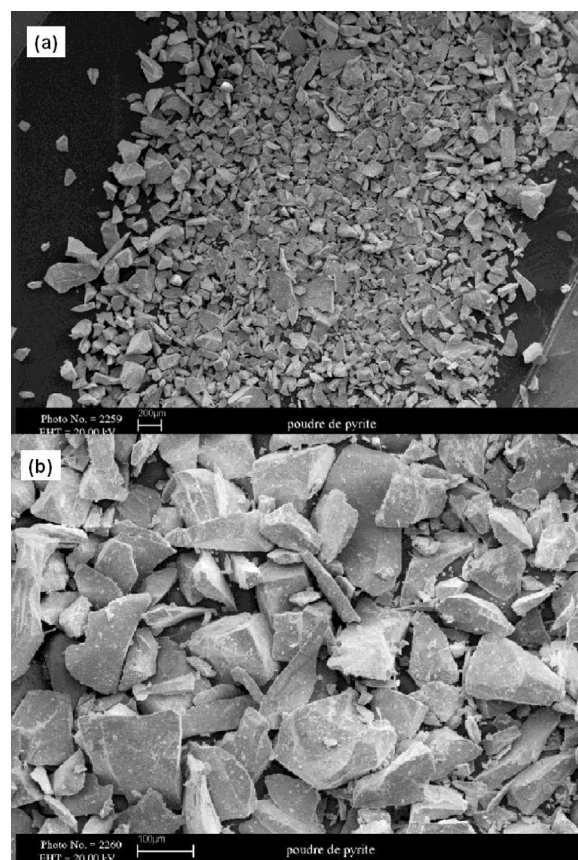


Fig. 1. SEM pictures of pyrite (FeS₂) as received. (a) General view; (b) details on the grain size.

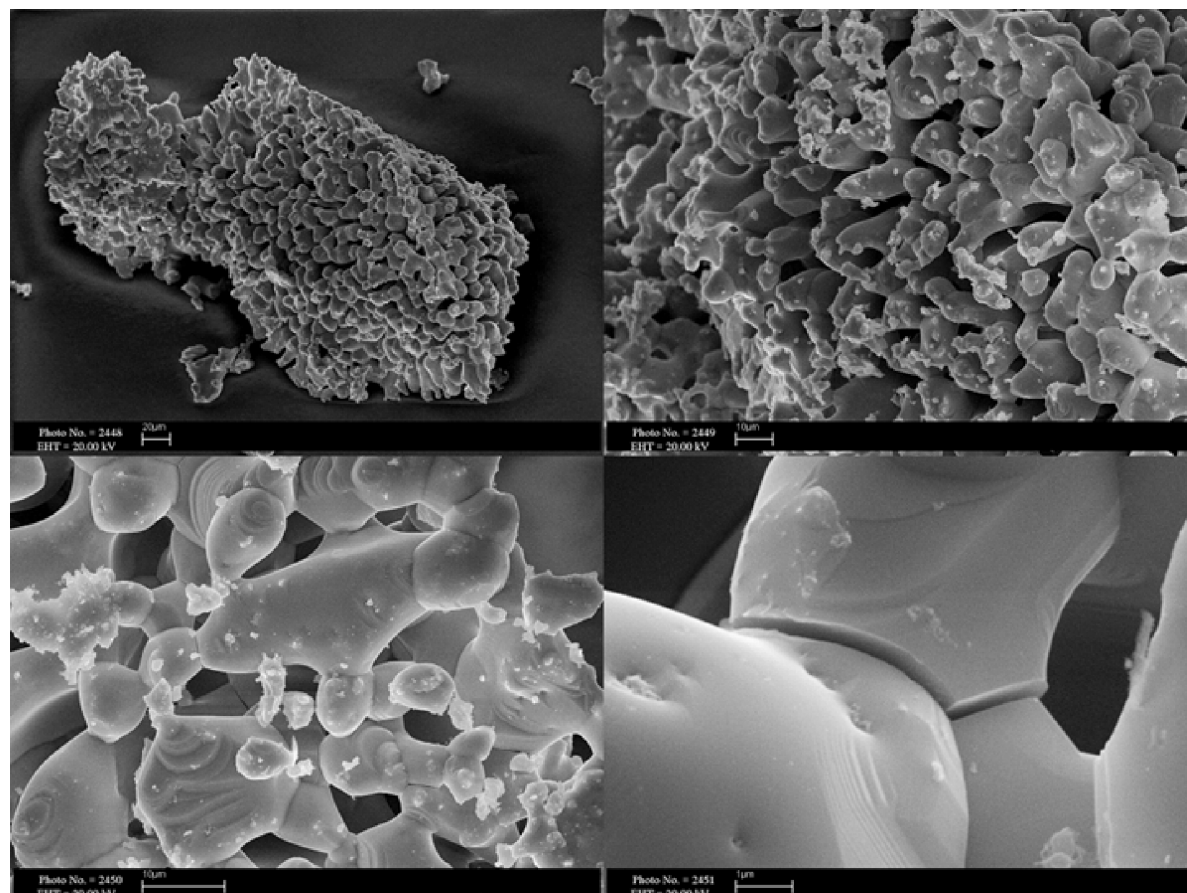


Fig. 2. SEM pictures of pyrite (FeS₂) decomposed under helium at 600 °C.

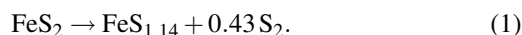
Table 1. Elemental analysis for iron, sulfur, oxygen and hydrogen in FeS₂ samples.

Element	Content (wt%)	Technique
Fe	45.3 ± 1.8	ICP-AES
S	56.8 ± 5.7	Carbothermal oxidation
O	1.5 ± 0.4	Carbothermal oxidation
H	15 ppm	Carbothermal oxidation

Iron, sulfur, oxygen and hydrogen contents were determined to evaluate impurity level of the FeS₂ sample. The values and techniques used are summarized in Table 1. The pyrite composition was found to be close to that of FeS_{1.98}, i. e. slightly sulfur-deficient. In addition to the pyrite phase, a hydrated sulfate phase, FeSO₄ · 9H₂O was evidenced by means of XRD. Sulfates are generally observed at the surface of FeS₂, even on fresh synthetic pyrite [29]. Their decomposition leads to the formation of Fe₂O₃ and contributes to the potential peak usually observed at the beginning of the battery discharge (Fig. 1).

3.2. FeS₂ Thermal Stability

Under inert atmosphere pyrite decomposes progressively into pyrrhotite, FeS_{1.14}, and sulfur gas according to [3]



During its thermal decomposition sulfur gas is released and this leads to a porous structure at the outer surface of the pyrite grains (Fig. 2). Although the kinetics is decreased in molten salts, in the pure molten LiCl-KCl eutectic free of oxides, pyrite decomposes into pyrrhotite and sulfur escapes as well.

Under a flow of inert gas, the sulfur gas arising from the thermal decomposition of pyrite is continuously removed from the interface FeS₂/FeS_{1.14} where the reaction takes place. Therefore the equilibrium FeS₂/FeS_{1.14} given by (1) is shifted to the right-hand side by promoting the evacuation of the sulfur gas.

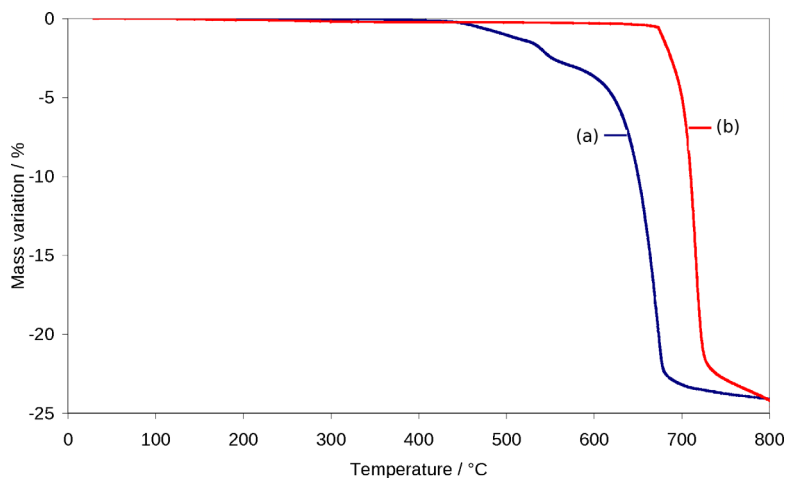


Fig. 3. TGA traces of pyrite samples under helium atmosphere (a) and in the LiCl-KCl eutectic (b).

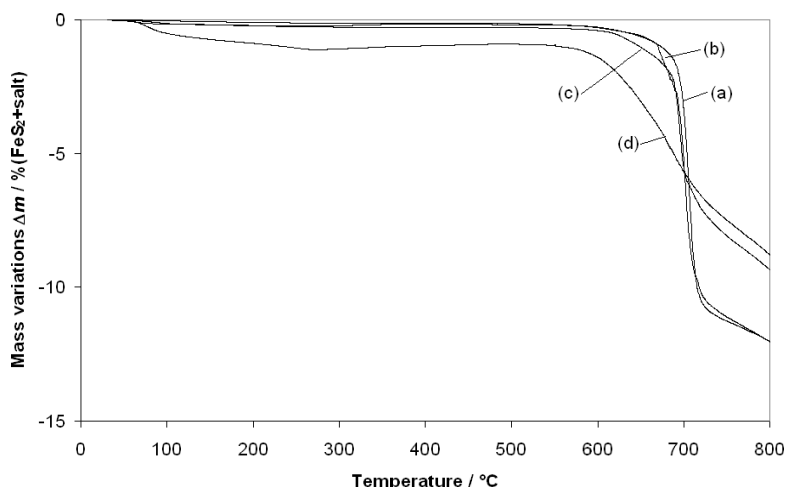


Fig. 4. Mass variations of samples of pyrite in molten salt (50:50 wt%) containing different levels of oxide versus the temperature. (a) 1 mol%; (b) 2 mol%; (c) 5 mol%; (d) 10 mol%.

When the pyrite grains are embedded in the liquid molten salt the situation differs. To some extent the sulfur gas is blocked in the tortuosity of the freshly produced porous layer of pyrrhotite. In this case, the sulfur partial pressure at the interface FeS₂/FeS_{1.14} increases. The equilibrium FeS₂/FeS_{1.14} is shifted towards the left-hand side and the decomposition temperature of pyrite increases. In Fig. 3 the mass variations of pyrite samples under helium at atmosphere and in the molten LiCl-KCl eutectic for a heating rate of 10 °C min⁻¹. This is clearly evidenced by comparing the TGA traces. The decomposition temperature of pyrite in the molten LiCl-KCl eutectic is approx. 75 °C (measured from the peak of the TGA derivative curve) higher than it is under helium gas. In the pure LiCl-KCl eutectic (without oxides or hydroxides) the mass loss is similar to that observed under helium gas. This im-

plies that no chemical reaction between the molten salt and the released sulfur gas happened. In this sense the thermal decomposition of pyrite in the pure LiCl-KCl eutectic and under helium gas could be considered as the same. XRD analysis of the reaction product confirmed this by the production of only pyrrhotite.

3.3. Effect of Oxide Dissolved in the Electrolyte

A weight fraction up to 10% of Li₂O was added to the molten phase. Figure 4 shows the mass variations versus temperature curves for different Li₂O concentrations in the electrolyte. For a low level of oxide (< 2 mol%), the curves are similar to that observed under inert gas. For higher oxide levels (5 and 10 mol%), the shape of the curves is significantly modified. Above 580–600 °C, pyrite starts to react with the oxide-

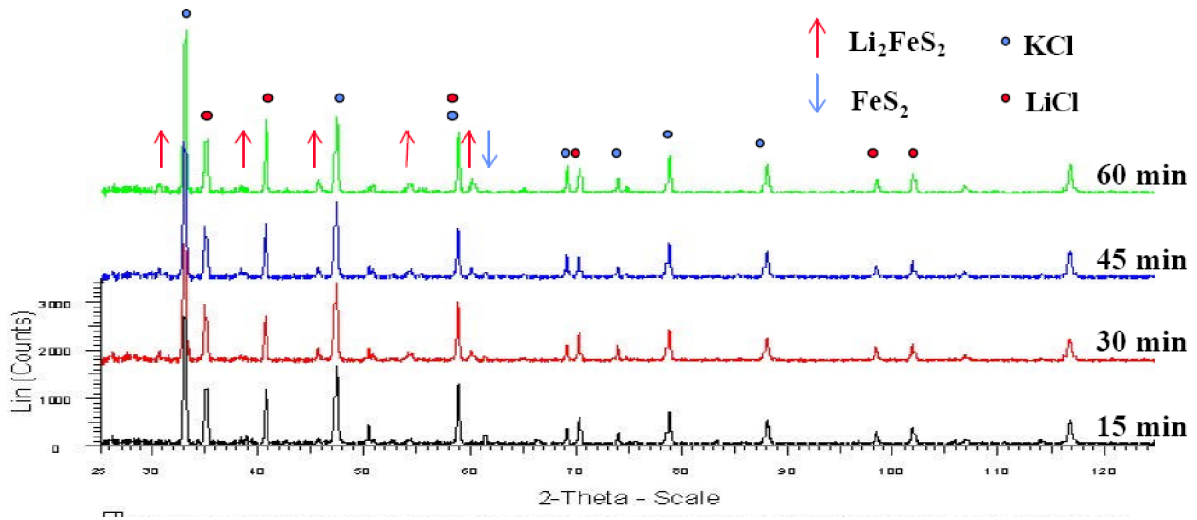
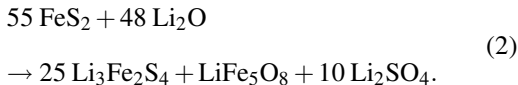


Fig. 5. XRD patterns of decomposition products of FeS₂ exposed to molten LiCl-KCl (10 wt% Li₂O) at 600 °C for 15 min, 30 min, 45 min, 60 min.

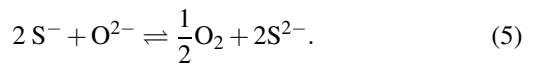
containing electrolyte and some weight losses are observed. At 680 °C the rest of unreacted pyrite decomposes into pyrrhotite independently of the Li₂O concentration. The samples used for TGA measurements were dissolved in water. A dark green-coloured solution was obtained. It indicates that the expected phase Li₃Fe₂S₄ is dissolved in water while leaching the salt phase. For a Li₂O content of 10 wt% some isothermal cycles were carried out for 15, 30, 45 and 60 min which are typical durations of thermal battery life times. After the annealing procedure the sample was cooled and ground for XRD analysis. Figure 5 shows the corresponding diffraction patterns. With the reaction duration the XRD peak intensity for pyrite decreases whereas new peaks are detected after 15 min. However, for longer reaction times, no significant increase of the peak intensity is observed; likely the reaction takes place in the first minutes. Similar fast reaction kinetics has already been evidenced for the formation of Li₃Fe₂S₄ during the cathode activation of the battery when lithium oxide is used to suppress the initial voltage spike. These new peaks are ascribed to the formation of Li₂FeS₂ although the quaternary phase diagram proposed by Aselage and Hellstom [17] suggested the formation of Li₃Fe₂S₄, Li₂SO₄ and LiFe₅O₈ according to



However, the XRD analysis does not sustain this mechanism. In order to explain the formation of the Li₂FeS₂ phase the following mechanism is suggested: Pyrite would progressively decompose at high temperature according to (1). In addition pyrrhotite and pyrite may also dissolve as sulfides in the LiCl-KCl eutectic [30]. The dissolved sulfides can react with the sulfur gas [31] arising from the thermal decomposition of pyrite to produce dissolved sulfites according to



Considering the oxidation potentials of the redox systems of dissolved oxides [32] and sulfur-based species [33], sulfites would be reduced by oxides according to



This would be supported by the work of Delarue [34] who studied dissolved sulfides in the LiCl-KCl eutectic even in the presence of oxides. He showed that the sulfides are not stable in the presence of oxides. In this case the formation of sulfides in the LiCl-KCl eutectic would be enhanced and may further react with the remaining pyrrhotite to form the phase Li₂FeS₂ according to



However, no experimental determinations can sustain the mechanism proposed as it involves numerous high temperature complex chemical equilibria. In addition, quantitative predictions would be somewhat hazardous as the equilibrium constants of the reactions described by (3), (4) as well as (5) are not known. But it should be emphasized that the proposed reaction pathway is consistent with previous investigations.

4. Conclusions

This work showed that the decomposition temperature of pyrite in molten salts shifts to higher temperatures as the S₂ gas is repressed by the liquid phase. For low lithium oxide contents the stability of pyrite remains unchanged. However, for higher contents the

decomposition temperature of pyrite decreases by approx. 100 °C. In addition the compound Li₂FeS₂ as reaction product was evidenced, and a mechanism was proposed to explain the formation of this unexpected phase.

Acknowledgement

The financial support of this project by CEA Le Ripault, LEPMI/INP Grenoble and ASB-Aerospatiale Batteries is deeply acknowledged. The author wishes to thank Jean-Claude Poinet (LEPMI/INP Grenoble), Jean-Yves Poinso (CEA Le Ripault) and Serge Schoeffert (ASB-Aerospatial Batteries) for their continuous support during the course of this project. Special thanks are due to Ronald Guidotti for his valuable comments to improve the document.

- [1] R. A. Guidotti and P. J. Masset, *J. Power Sources* **161**, 1443 (2006).
- [2] P. J. Masset and R. A. Guidotti, *J. Power Sources* **164**, 397 (2007).
- [3] P. J. Masset and R. A. Guidotti, *J. Power Sources* **177**, 595 (2008).
- [4] I. C. Hoare, H. J. Hurst, W. I. Stuart, and T. J. White, *J. Chem. Soc. Faraday Trans. 1* **84**, 3071 (1988).
- [5] G. Santarini, *Electrochim. Acta* **27**, 495 (1982).
- [6] F. C. Mrazek and J. E. Battles, *J. Electrochem. Soc.* **124**, 1556 (1977).
- [7] B. Tani, F. Mrazek, J. Faber, and R. Hitterman, *J. Electrochem. Soc.* **133**, 2644 (1986).
- [8] Z. Tomczuk, B. Tani, N. C. Otto, M. F. Roche, and D. R. Vissers, *J. Electrochem. Soc.* **129**, 925 (1982).
- [9] Z. Tomczuk, S. K. Preto, and M. F. Roche, *J. Electrochem. Soc.* **128**, 760 (1981).
- [10] S. K. Preto, Z. Tomczuk, S. von Winbush, and M. F. Roche, *J. Electrochem. Soc.* **130**, 264 (1983).
- [11] G. Barlow, Investigation of Mechanism for Capacity Loss in Iron Disulfide Electrodes in High-Temperature Lithium-Alloy / Metal Sulfide Batteries, Final Report to Lawrence Berkeley Laboratory, University of California, Berkeley, CA 1986.
- [12] P. J. Masset, J.-Y. Poinso, S. Schoeffert, and J.-C. Poinet, Proceedings of the 39th International Power Sources Conference, Cherry Hills, Philadelphia, NJ, USA 2002, p. 246.
- [13] P. J. Masset, V. Frotté, J.-Y. Poinso, and J.-C. Poinet, *J. Power Sources* (in preparation).
- [14] J. P. Pemsler, R. K. F. Lam, J. K. Litchfield, S. Dallek, B. F. Larrick, and B. C. Beard, *J. Electrochem. Soc.* **137**, 1 (1990).
- [15] P. S. Thomas, D. Hirschauen, R. E. White, J. P. Guerbois, and A. S. Ray, *J. Therm. Anal. Cal.* **72**, 769 (2003).
- [16] R. A. Guidotti, Patent US 4,731,307, 1988.
- [17] T. L. Aselage and E. E. Hellstrom, *J. Electrochem. Soc.* **134**, 1932 (1987).
- [18] R. A. Guidotti, F. W. Reinhardt, and W. F. Hammett, Sandia report SAND85-1737 (1988).
- [19] R. A. Guidotti and F. W. Reinhardt, Proceedings of the 2nd Annual Battery Conference on Applications and Advances, Long Beach, CA, USA 1986, p. 229.
- [20] K. Gourishankar and E. J. Karell, *Light Met.* **1123** (1999).
- [21] K. Gourishankar, L. Redey, and M. Williamson, *Light Met.*, 1075 (2002).
- [22] G. K. Johnson, *Light Metals* (Eds. B. Mishra and W. A. Aerill), The Minerals, Metals & Material Society, Warrendale, PA 1994, p. 199.
- [23] N. M. Barbin and V. N. Nekrasov, *Electrochim. Acta* **44**, 4479 (199).
- [24] Y. Kaneko and H. Kojima, *Denki Kagaki* **42**, 304 (1974).
- [25] T. L. Aselage and E. E. Hellstrom, *J. Electrochem. Soc.* **134**, 1932 (1987).
- [26] T. L. Aselage and E. E. Hellstrom, *J. Electrochem. Soc.* **134**, 1929 (1987).
- [27] C. H. Liu and L. P. Pioto, *J. Chem. Eng. Data* **14**, 83 (1969).
- [28] R. Sridhar, C. E. Johnson, and E. J. Cairns, *J. Chem. Eng. Data* **15**, 244 (1970).
- [29] J. P. Pemsler, R. K. F. Lam, J. K. Litchfield, S. Dallek, B. F. Larrick, and B. C. Beard, *J. Electrochem. Soc.* **137**, 1 (1990).
- [30] R. A. Sharma and R. N. Seefurth, *J. Electrochem. Soc.* **131**, 1084 (1984).

- [31] D.M. Gruen, R.L. McBeth, and A.J. Zielen, *J. Am. Chem. Soc.* **93**, 6691 (1971).
- [32] Y. Kansaki and M. Takahashi, *J. Electroanal. Chem. Interfacial Electrochem.* **58**, 339 (1975).
- [33] J.R. Birk and R.K. Steunenberg, *Adv. Chem. Ser.* **140**, 186 (1975).
- [34] G. Delarue, Ph.D. thesis, University of Paris 1960.